POSTPRINT version of Supercond. Sci. Technol. **35** (2022) 045012 https://doi.org/10.1088/1361-6668/ac5339

Transport and structural properties of MgB_2/Fe wires produced by redesigning internal Mg diffusion process

Hakan Yetiş[1], Doğan Avcı[1], Fırat Karaboğa[2], Canan Aksoy[3], Daniel Gajda[4], Elena Martínez[5], Fatih Mehmet Tanyıldızı[6], Andrzej Zaleski[4], Michal Babij[4], Lan Maria Tran[4], Luis Alberto Angurel[5], G F De La Fuente[5] and İbrahim Belenli[1]

[1] Physics, Bolu Abant İzzet Baysal University (BAİBU), Bolu, Turkey
[2] Mehmet Tanrikulu Vocat. Sch. Hlth. Serv., BAİBU, Bolu, Turkey
[3] Electronics and Communication Engineering, Karadeniz Technical University, Trabzon, Turkey
[4] Institute of Low Temperature and Structure Research PAS, Wroclaw, Poland
[5] Instituto de Nanociencia y Materiales de Aragón (CSIC-Universidad of Zaragoza), Zaragoza, Spain
[6] Electrical and Electronics Engineering, BAİBU, Bolu, Turkey

E-mail: yetis_h@ibu.edu.tr

Received 14 January 2022, revised 8 February 2022
Accepted for publication 9 February 2022
Published 1 March 2022

Abstract

We report transport, electromechanical, and structural properties of single core MgB_2/Fe wire produced using a new fabrication method, called designed IMD process, which relies on the use of non-stoichiometric Mg + B pellets with excess Mg in place of a central Mg rod used in the standard internal Mg diffusion (IMD) method. Structural analysis revealed the successful formation of a porous MgB_2 structure in the center and a dense circular MgB_2 layer surrounding this structure in the designed-IMD wire. Fast transport I –V measurements showed that the designed IMD method increased engineering critical current density (J_e) up to twice that of the IMD wires in self-field. The central porous MgB_2 structure shared the applied current and indirectly behaved as an internal stabilizer against quench damage at high applied currents.

Keywords: MgB_2 wire, IMD, PIT, boron

1. Introduction

MgB_2 with 39 K critical temperature is a suitable material for the realization of cryogen-free magnetic resonance imaging (MRI) magnets, as it can be wired in a viable metallic sheath and operated above 4.2 K. However, the operating cost of MgB_2 wire should be lowered compared to the niobium-titanium (NbTi), commonly used in commercial MRI systems, and therefore LHe-free cryocooling systems are needed to be developed for the realization of MgB_2 MRI magnets [1-5]. Another requirement for the construction of a large MgB_2 magnet is that kilometers of superconducting wire must be produced. The *in-situ* MgB_2 wires produced by the powder-in-tube (PIT) method, in which the magnesium and boron (Mg + B) powder mixture is encased in a suitable metallic tube, are now fabricated in km length scales [6, 7]. The internal magnesium diffusion method, which enables a significantly higher in-field critical current density (J_c) than the PIT method, is more advantageous in terms of using MgB_2 instead of NbTi in the MRI magnet [8 – 11]. However, the J_e in IMD wires is lower than that of PIT wires because a

large hole is formed in the center of IMD wire due to diffusion of the central Mg rod into the surrounding boron during heat treatment [11-16]. The core uniformity is also challenging in production of long IMD wires due to the variations in the packing density of boron powder along the IMD wire, leading to changes in the superconducting properties after heat treatment. Therefore, improving the longitudinal uniformity and J_e in IMD wires is essential for large-scale applications [11, 16 - 21].

Superconducting joining is required to operate MRI magnets in permanent current (PC) mode because an ultra-stable magnetic field with a decay rate of < 0.1 ppm h^{-1} is required for high resolution images. MRI magnet construction using a superconducting MgB_2 wire is conceivable by joining individual coils in series but a very low joint resistance is needed in terms of heat generation [22, 23]. Recent studies have been showing that the joint resistance as low as 10^{-15} Ω is achieved in joining of unreacted MgB_2 wires [4, 24 - 27]. However, reliable superconducting joints have not yet been fully optimized, especially for reacted MgB_2 wires [11, 28 - 30].

In this study, standard-IMD, powder-IMD, and designed-IMD wires were fabricated using a multi-pass cold drawing process at room temperature [31]. Mg/B pellets with excess Mg and Mg in powder form were used in place of a central Mg rod in the designed and powder-IMD wires, respectively. In this way, the role of Mg in different forms was explored in terms of internal diffusion of Mg in IMD wires. For designed-IMD wire, a central porous MgB_2 structure with a surrounding dense MgB_2 layer was formed to take advantage of both the J_e of PIT and the excellent J_c of IMD processes. The central porous MgB_2 in the designed- IMD wire is also advantageous in terms of superconducting joining because it provides a larger MgB_2 contact surface than that of the standard-IMD wire having a large hole.

Additionally, there are not many studies on the electromechanical properties of single core IMD MgB_2 wires [32 - 35]. In this study, degradation in critical current (I_c) as a function of bending diameter was studied for different wire pieces.

2. Experimental Details

The wire called S1 was produced using the designed-IMD method with the filling steps mentioned below. First, amorphous nano-boron powder (98 % purity, < 250 nm size) was filled into the space between the pre-centered 6.6 mm diameter steel rod and the iron tube by hand compression. The steel rod was used as a guide to obtain a boron layer at the inner surface of the iron (Fe) tube. After filling the Fe tube with boron powder, the steel rod was gently pulled out. Mg/B pellets with 6.4 mm diameter were prepared by pressing $Mg_{0.052} + B_{0.039}$ powder mixture (95 – 97 %, < 1 μm, semi-amorphous boron; 99 %, 325 mesh magnesium) under pressure of 305 MPa. Finally, the pellets were placed one by one into the central hole left behind by the removal of the steel rod (see Figure 1). S2 is a standard-IMD wire in which the Mg rod with 4.6 mm diameter was fixed in the center of the Fe tube and the amorphous nano-boron powder was filled into the empty region between the Mg rod and the Fe tube by hand pressing.

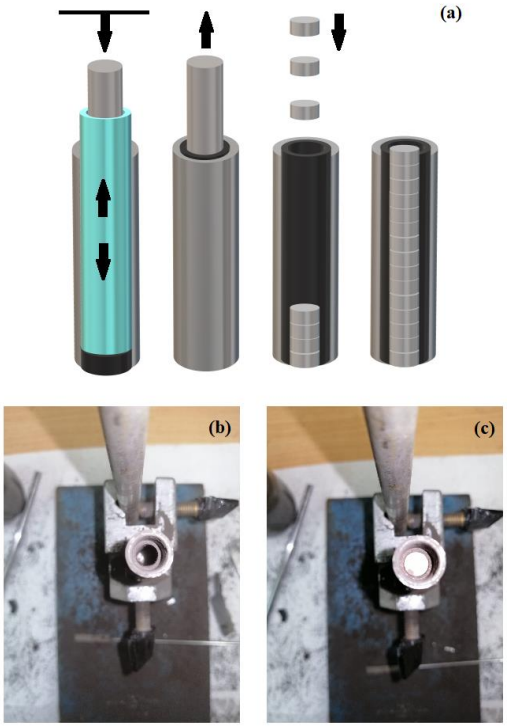

Figure 1. (a) Schematic and (b) – (c) real images for *in situ* designed IMD filling process.

S3 wire was produced using the magnesium powder method [36], in which Mg powder was used instead of Mg rod. The diameter of the space in the center for filling the Mg powder was again 6.4 mm. Thorough this arrangement, we achieved MgB_2 ring layer thicknesses which were not much different in S1 and S3 after the reaction as represented in Figures 2(a) and 2(e), respectively. Mg powder was not compressed in order not to distort the surrounding boron layer. The initial iron tubes with outer/inner diameter 12/9 mm were used for all samples. All composites were brought to round wire form by cold drawing from 12 mm to 0.81 mm with several intermediate heat treatments. The wire pieces of 300 mm length were synthesised at 650 °C (5 °C/min ramping rate) for 4 h under argon atmosphere to form MgB_2 phase (see Figure 2). The fact that the wire pieces were 300 mm long and their ends were closed by pressing prevented the loss of magnesium from the wire ends during the heat treatment. Pre-tested reacted straight wire samples of 25 mm length were bent to a certain bending diameter at room temperature, and degradation in I_c was surveyed by current-voltage measurements on released wires at 25 K using a gas contact closed-cycle cryostat (Cryo-Industries) system with a

superconducting magnet up to 7T [37]. The straight wire pieces were bent to different diameters of 350 mm, 300 mm, 250 mm, 200 mm, 175 mm, 150 mm, 125 mm and 100 mm for all samples.

The fast $I - V$ measurements in self-field were performed on samples approximately 25 mm long in vacuum, cooled by conduction from both current contacts, which were thermally in contact (and electrically insulated) to a copper block anchored to the second stage of a cryocooler. A thermometer was attached to one of the current contacts, a heater on the copper block and a Lakeshore temperature controller were used to control the temperature of the sample. Current linear ramps for 1 s were used to avoid heating the sample during the measurements.

The in-field critical current (I_c) measurements were made at the Institute of Low Temperatures and Structural Bdań PAN in Wrocław. The I_c measurements in liquid helium were made by using Bitter magnet of 14 T and a direct current (DC) source from 0 A to 150 A. On the other hand, the measurements of I_c at 20 K and 25 K were made using the Oxford Instruments Susceptometer, e.g. temperature range 2- 350 K, magnetic fields up to 9T and DC range from 0 A to 150 A. All I_c measurements were made in a perpendicular magnetic field. The critical currents were determined on the basis of the 1 μm/cm criterion.

A scanning electron microscope (FEI, Quanta FEG 250) with the accelerating voltage of 30 kV was used to investigate the surface morphology of the Fe/MgB_2 wires.

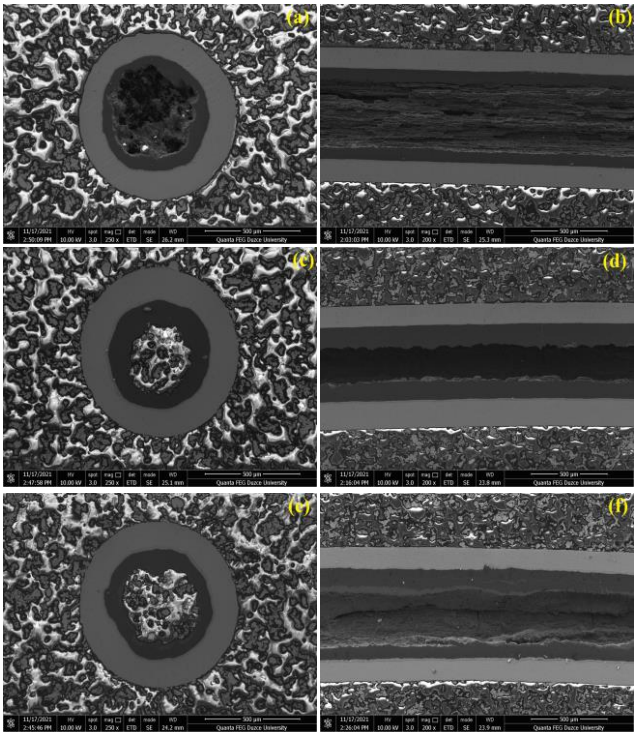

Figure 2. SEM images for cross-sectional and longitudinal views of (a) – (b) S1, (c) – (d) S2, and (e) – (f) S3 samples, after synthesis.

3. Results

3.1 Transport measurements with fast current ramp in self-field

Figures 3(a) – 3(c) show the transport measurement results for S1, S2, and S3 samples at various temperatures above 30 K. The I_c values in the self-field were determined from the $I - V$ characteristic curves using 1 μV/cm criterion. In the experiments, we first set the temperature to 36 K. After the temperature stabilized, the maximum current of the ramps was gradually increased to reach the I_c value. Later, the temperature was set to a lower value and the process was repeated. In the case of sample S1, although the voltage increases very sharply after achieving the I_c value at higher currents (see Figure 3a), no damage is observed and this sample had the same I_c value in repeated measurements at all temperatures. However, for the other samples the behavior at high currents is different. An example of this effect is shown in Figure 3(b), corresponding to sample S3 at 34 K. In the first ramp up to 90 A, not appreciable voltage (above the noise level) was observed (curve blue in the figure). Nevertheless, at high applied currents, the quenching effect caused the current not to increase any further and reflected itself as current oscillations through the end of current ramping. Beyond that, the S3 sample was completely damaged when it was re-measured at 34 K. The obtained results suggested that the quench triggered outside the zone between the voltage taps. Similar but relatively weak quenching effect on I_c was also observed for S2 sample at 32 K. In our opinion, the quench occurs either at the ends of the current contacts or in the current contact itself and propagates to the rest of the sample. Although the current was ramped in 1s, quench was not tolerated, and thus S2 and S3 samples were damaged at high applied currents.

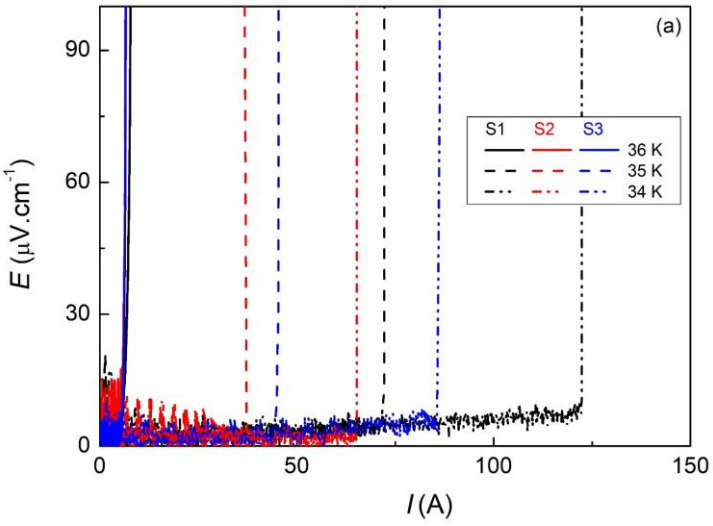

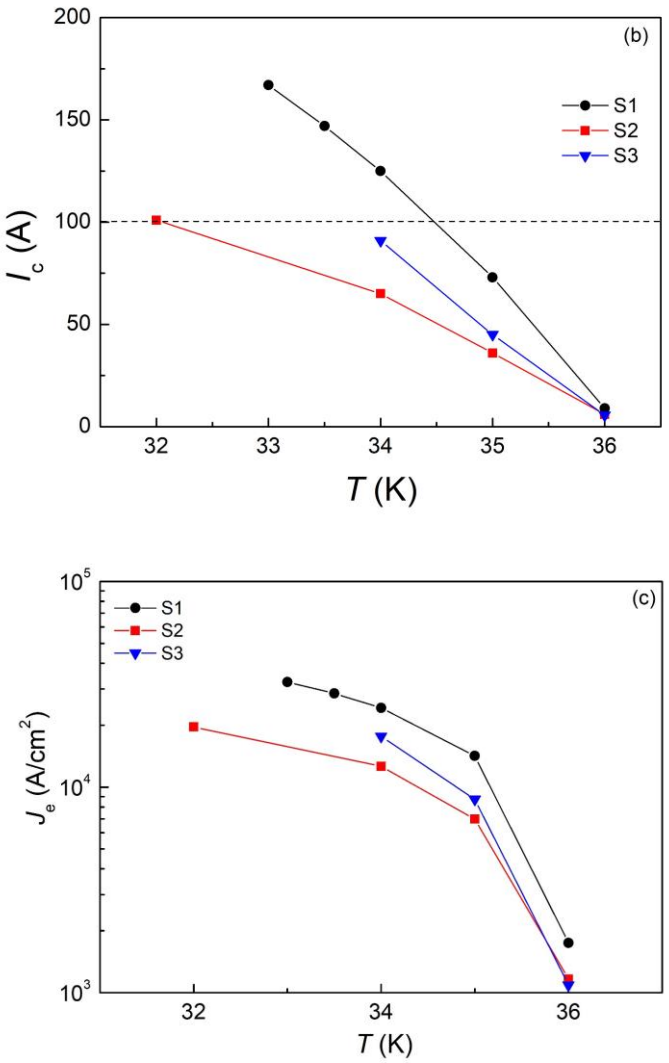

Figure 3. (a) Electric field – current (E – I) characteristics for S1, S2, and S3 wires in self-field. (b) Temperature dependent transport critical current (I_c) behaviour of S1, S2, and S3 samples in self field. (c) J_e – T curves for all samples. In Figure 3(a), solid, dashed, and dashed-dot lines represent the 36 K, 35 K, and 34 K, respectively.

.

The results indicated that Fe-sheathed IMD wires had quenched even below their critical currents when they were not properly stabilized (see Figure 4). On the other hand, the designed IMD wire allowed applying relatively higher currents without a direct quench damage and had a higher J_e than that of the IMD wires in self-field as shown in Figures 3(b) and 3(c). It seems that, at least for these three wires, IMD wires are more prone to quenching as previously stated in the study of Kováč *et al*. [38]. We suggest that the low thermal stability of of Fe/MgB_2 IMD wire could be improved by IMD/PIT hybridization against the negative effect of quench power. This is because we consider that the applied current is shared between the central porous MgB_2 core and dense MgB_2 layer in S1 and the low thermal stability of iron is somewhat compensated in this way.

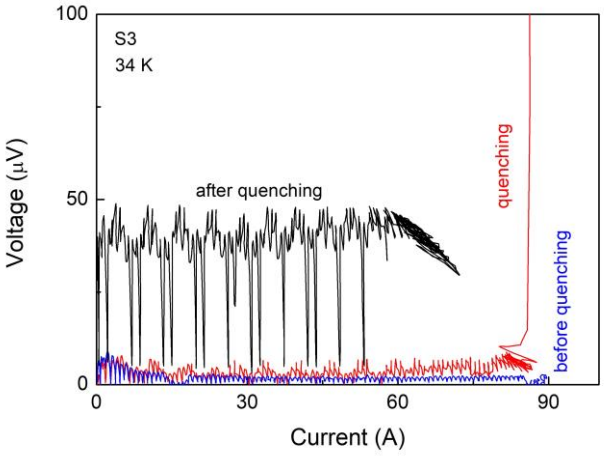

Figure 4. Quench development for S3 wire at 34 K in self-field

3.2 Direct current (DC) transport measurements under external magnetic field

DC transport measurements for I_c were made at 4.2 K, 20 K, and 25 K under various external magnetic fields for all samples as shown in Figure 5. We observed that samples S1 and S3 had similar critical currents at 20 and 25 K, although I_c values in moderate fields (about 4 – 6 T) were slightly higher for S1 than S3. However, the S2 sample presented the highest I_c values at 4.2 K among the analyzed samples, although very close to those of the S1 wire. In contrast, S2 had the lowest values at 25 K in all fields. Therefore, we observed that, generally, S1 sample was only capable of carrying as much current as S2 and S3 wires under external magnetic fields. It seems that the external field suppresses the superconductivity in the porous MgB_2 core of S1, and thus the current is not shared by the central core and is carried only by the thin MgB_2 layer of S1, resulting with I_c value close to that of S2 and S3 wires. We consider that a better high field pinning can be achieved in the porous MgB_2 core of S1 with a combination of some other methods such as carbon doping. For instance, our previous study showed that Mg could form a layered (lamellar) structure that allows J_c and B_{irr} to be increased [39].

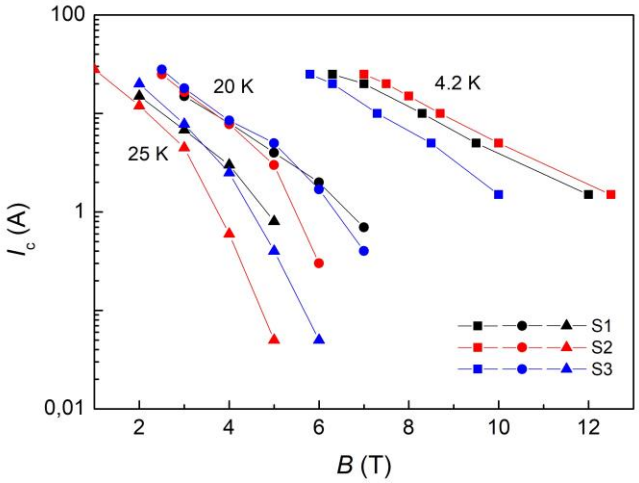

Figure 5. I_c vs. B characteristics for S1, S2, and S3 wires.

The quench may be initiated due to the interface resistance of iron-boride phases between the Fe sheath and core in all wires. The highly reactive nano amorphous boron reacted with iron sheath even at relatively low synthesis temperatures of 650 ºC [40]. This is because quenching became more pronounced and limited to apply higher currents to our thin wires in all temperatures, when the direct current was not transferred fast to the samples.

3.3 Electromechanical (bending strain) measurements

Transport measurements for I_c of straight and bent wires were performed at 25 K under magnetic fields of 4.8 T, 5.0 T and 4.7 T for S1, S2, and S3 wire pieces, respectively. The magnetic fields were adjusted to equalize the I_c values of the samples [37]. Figure 6 shows the normalized critical currents (I_c / I_{c0}) as a function of bending strain (ε_B), calculated by using the formula $\varepsilon_B = \varphi / d$ where φ is the wire diameter (0.81 mm) and d is the bending diameter ranging from 100 mm to 350 mm. I_{c0} and I_c are the critical currents of the wires in their straight and bent forms, respectively. The critical current measurements were made on different reacted short wire pieces of 25 mm length taken from different parts of the wires in order to check the homogeneity of the wires. We found that bending was tolerated up to 0.46 % for S1 and S2 samples and 0.40 % for S3 sample.

Figures 7(a) to 7(f) show the optical microscopy images of bent S1, S2, and S3 samples. The bending diameters at which the first breaks occur are 150 mm for S1 and S2 samples and 175 mm for S3 sample. The longitudinal views of the wire samples in Figures 7(a), 7(c), and 7(e) reveal the appearance of the structural micro cracks causing the initial degradation in I_c. The crack formation occurred in three places on the stretched side of the core in each sample, where the compressed side did not yield any crack. Figures 7(a), 7(c) and 7(e) show the thickness values for the dense MgB_2 layer (orange color) and Figures 7(b), 7(d) and 7(f) reveal the width of the cracks in each sample. The porous MgB_2 structure formed in the center of the S1 wire cannot be seen with the optical microscopy, but this structure is exhibited in the SEM images given in Figures 2(a) and 2(b). S3 has an inhomogeneous core structure and the core thickness is

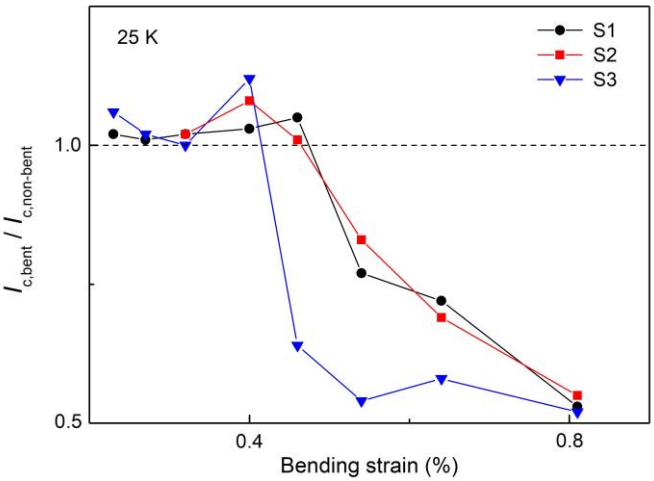

Figure 6. Normalized current vs. Bending strain tolerance characteristics for S1, S2, and S3 wires. The maximum applied current is 1 A. Each reacted straight wire piece was bent to a certain bending diameter at room temperature.

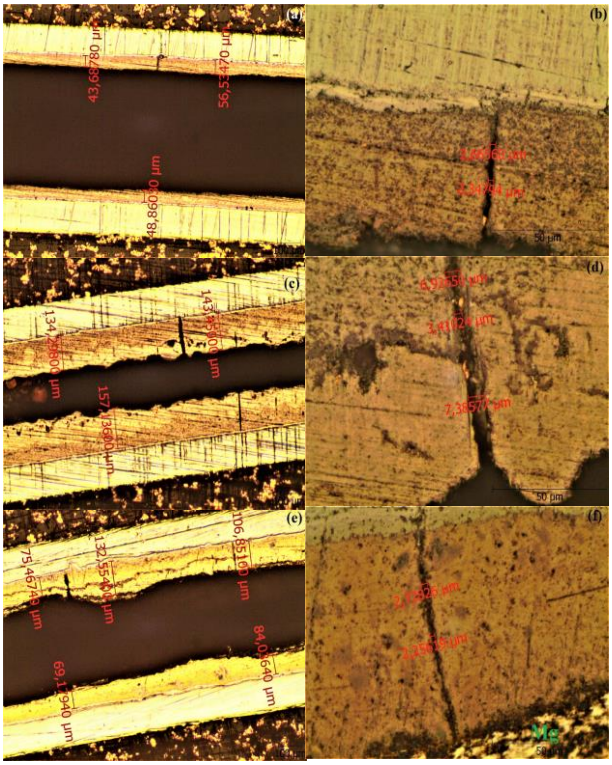

Figure 7. Optical microscopy images for 5× and 50× magnifications taken from (a) – (b) S1, (c) – (d) S2, and (e) – (f) S3 wires.

relatively smaller than that of the S2 sample. We consider that the MgB_2 core thickness is a critical factor in IMD wires. This is because a thick MgB_2 core of S2 provided a better bending strain tolerance than that of S3, but wider cracks were formed in the S2 sample, which has the thickest MgB_2 core, than in the S1 and S3 samples. S3, with a large mid-cavity, contains significant amounts of unreacted Mg near the interior of the MgB_2 core. This can be considered as the cause of the longitudinal non-uniformity in S3 wire and formation of longitudinal cracks under bending as seen in Figure 7(e). On the other hand, S1 sample has a fairly good longitudinal uniformity although it has the thinnest MgB_2 ring layer among the samples. It seems that the complete diffusion of Mg towards the surrounding nano boron layer in S1 was achieved by using semi-crystalline boron powder, having low reactivity with Mg, in the center [41, 42].

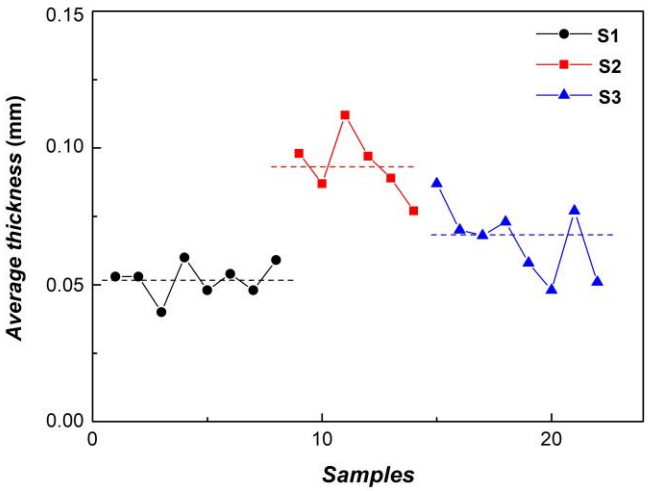

Figure 8. Average MgB_2 core thicknesses for various S1, S2, and S3 wires.

Figure 8 shows the average MgB_2 layer thickness values obtained from various S1, S2 and S3 samples. MgB_2 core thicknesses were determined by averaging the thicknesses measured from at least ten different locations along the lateral MgB_2 cores. It was found that S2 had the largest MgB_2 layer with thickness of 93 μm, while S1 had the thinnest layer about 50 μm on average. The designed IMD method enabled to obtain a more uniform MgB_2 core than IMD wires as seen in Figure 8. Apparently, the variations in MgB_2 layer thickness are not totally avoidable as the Mg metal in powder or rod form was being elongated through the boron powder.

4. Conclusions

In this study, a new type of single-core IMD MgB_2/Fe wire with a diameter of 0.81 mm was produced and experimentally characterized. In this new proposed method, Mg/B pellets with excess Mg were used in place of the central Mg rod normally used in standard IMD method. Structural analysis demonstrated the successful fabrication of the designed-IMD wire (S1) characterized by a uniform and dense annular MgB_2 layer around a central porous MgB_2 core. By comparison, a standard-IMD wire (S2) and a powder-IMD wire (S3), in which Mg powder was used instead of Mg rod, were also fabricated and characterized. The normalized I_c vs. bending strain measurement results revealed that the designed-IMD wire had the critical bending stress tolerance of 0.46 % which is the same as the S2 wire and is better than that of S3. Here, S2 wire has an MgB_2 layer thickness of about 2.5 times thicker than that of the S1. According to the fast $I - V$ measurement results, S1 carried the highest current without quenching among the samples and had an I_c value of 167 A at 33 K in the self field. The porous MgB_2 structure in S1 core shares the applied current, increasing J_e compared to S2 and S3. In this way, the porous MgB_2 structure in S1 core also indirectly acts as a stabilizer against the quench damage. It was observed that S2 and S3 IMD wires were more prone to quench and needed to be properly stabilized due to a lower thermal stability of Fe sheath. More importantly, formation of resistive iron boride (FeB, Fe_2B) phases became a more critical issue in terms of quench, when the direct current was not transferred fast enough to the samples. We consider that the designed IMD method deserves further investigations, especially for multifilament IMD wires and their joints, as it offers the advantages of uniformity, parametrization (i.e., the choice precursor material, carbon doping, MgB_2 layering size etc.) and higher J_e for IMD wires.

Acknowledgements

This work is funded by the Scientific and Technological Research Council of Turkey (TUBITAK) research project with grant number 119M288. E.M. acknowledges the financial support from MCIN/AEI/10.13039/501100011033 (project PID2020-113034RB-I00) and from Gobierno de Aragón "Construyendo Europa desde Aragón" (research group T54_20R). The use of Servicio General de Apoyo a la Investigación-SAI (Universidad de Zaragoza) is also acknowledged.

References

[1] Baig T, Yao Z, Doll D, Tomsic M and Martens M 2014 *Supercond. Sci. Technol.* **27** 125012
[2] Lvovsky Y, Stautner E W and Zhang T 2013 *Supercond. Sci. Technol.* **26** 093001
[3] Yao C, Ma Y 2021 *iScience* **24** 102541
[4] Patel D, Hossain M S A, See K W, Qiu W, Kobayashi H, Ma Z, Kim S J, Hong J, Park J Y, Choi S, Maeda M, Shahabuddin M, Rindfleisch M, Tomsic M, Dou S X and Kim J H 2016 *Supercond. Sci. Technol.* **29** 04LT02
[5] Iwasa Y 2017 *Supercond. Sci. Technol.* **30** 053001
[6] Baig T, Amin A A, Deissler R J, Sabri L, Poole C, Brown R W, Tomsic M, Doll D, Rindfleisch M, Peng X, Mendris R, Akkus O, Sumption M and Martens M 2017 *Supercond. Sci. Technol.* **30** 043002

[7] Tanaka H, Suzuki T, Kodama M, Koga T, Watanabe H, Yamamoto A and Michizono S 2020 *IEEE Trans. Appl. Supercond* **30** 6200105

[8] Takahashi M, Tanaka K, Okada M, Kitaguchi H and Kumakura H 2006 *IEEE Trans. Appl. Supercond*. **16** 1431–1434

[9] Ye S, Song M, Matsumoto A, Togano K, Takeguchi M, Ohmura T and Kumakura H 2013 *Supercond. Sci. Technol*. **26** 125003

[10] Ye S, Matsumoto A, Zhang Y and Kumakura H 2014 *Supercond. Sci. Technol*. **27** 085012

[11] Ye S and Kumakura H 2016 *Supercond. Sci. Technol*. **29** 113004

[12] Hur J, Togano K, Matsumoto A, Kumakura H, Wada H and Kimura K 2008 *Supercond. Sci. Technol.* **21** 032001

[13] Li G Z, Sumption M D, Susner M A, Yang Y, Reddy K M, Rindfleisch M A, Tomsic M J, Thong C J and Collings E W 2012 *Supercond. Sci. Technol.* **25** 115023

[14] Yetiş H, Karaboğa F, Avcı D and Belenli İ 2021 *Physica C* **581** 1353807

[15] Giunchi G, Ripamonti G, Perini E, Cavallin T and Bassani E 2017 *IEEE Trans. Appl. Supercond*. **17** 2761

[16] Ye S J, Matsumoto A, Togano K, Zhang Y C, Ohmura T and Kumakura H 2014 *Supercond. Sci. Technol.* **27** 055017

[17] Higashikawa K, Tatara H, Inoue M, Ye S, Matsumoto A, Kumakura H and Kiss T 2016 *IEEE Trans. on Applied Supercond* **26** 6200804

[18] Kováč P, Hušek I, Hain M, Kopera L, Melišek T and Berek D 2021 *Supercond. Sci. Technol*. **34** 095007

[19] Kováč P, Kopera L, Hain M, Martínez E, Kováč J, Melišek T, Berek D and Hušek I 2020 S*upercond. Sci.Technol*. **33** 085004

[20] Wang D, Xu D, Zhang X, Yao C, Yuan P, Ma Y, Oguro H, Awaji S and Watanabe K 2016 *Supercond. Sci. Technol*. **29** 065003

[21] Bovone G, Capra M, Bernini C, Loria F, Cetner T, Gajda D, Morawski A, Ballarino A, Hopkins S C, Tropeano M, Grasso G, Putti M, Ferdeghini C, Siri A S and Vignolo M 2020 *Super. Sci. Technol*. **33** 125003

[22] Patel D, Matsumoto A, Kumakura H, Maeda M, Kim S H, Liang H, Yamauchi Y, Choi S, Kim J H and Hossain M S A 2021 *Scripta Materialia* **204** 114156

[23] Patel D, Kim S H, Qiu W, Maeda M, Matsumoto A, Nishijima G, Kumakura H, Choi S and Kim J H 2019 *Sci. Rep*. **9** 14287

[24] Matsumoto A and Kumakura H 2018 *IEEE Trans. Appl. Supercond*. **28** 6200104

[25] Patel D, Matsumoto A, Kumakura H, Nishijima G, Maeda M, Kim S H, Choi S and Kim J H 2020 *Scripta Materialia* **178** 198–202

[26] Luo W, Huang Z, Cai X, Pan X, Linghu K, Wu Q, Nie R, Feng Q, Wang F, and Gan Z 2019 *IEEE Trans. Appl. Supercond*. **29** 6200805

[27] Xi D, Wang D, Xinwei C, Wang Q, Huang Z, Nie R, Yan G, Wang F and Gan Z 2021 *Supercond. Sci. Technol*. **34** 125009

[28] Li X H, Ye L Y, Jin M J, Du X J, Gao Z S, Zhang Z C, Kong L Q, Yang X L, Xiao L Y and Ma Y W 2008 *Supercond. Sci.Technol*. **21** 025017

[29] Ling J, Voccio J P, Hahn S, Qu T, Bascuñán J and Iwasa Y 2017 *Supercond. Sci. Technol*. **30** 024011

[30] Kim S H, Patel D, Maeda M, Kim M, Lee S H, Choi S and Kim J H 2021 *Supercond. Sci. Technol*. **34** 125003

[31] Sun L, Bai J, Xue F, Chu C and Meng J 2018 *Materials* **11** 602

[32] Nishijima G, Ye S J, Matsumoto A, Togano K, Kumakura H, Kitaguchi H and Oguro H 2012 *Supercond. Sci. Technol*. **25** 054012

[33] Kováč P, Hušek I, Melišek T, Kulich M and Kopera L 2016 S*upercond. Sci. Technol*. **29** 045002

[34] Kováč P, Hušek I, Rosová A, Melišek T, Kováč J, Kopera L, Schleiter J and Haessler W 2019 *Physica C* **560** 40-44

[35] Avcı D, Yetiş H, Karaboğa F, Akdoğan M and Belenli İ 2021 *J. Supercond. and Nov.Magn*. **34** 2121–2129

[36] Yetiş H, Avcı D, Karaboğa F, Gajda D, Akdoğan M and Belenli İ 2020 *Physica B* **593** 412277

[37] Tanaka H, Suzuki T, Kodama M, Nishijima G and Matsumoto A 2019 *IEEE Trans. Appl. Supercond*. **29** 8401104

[38] Kováč P, Hušek I, Pérez N, Rosová A, Berek D, Gelišuaková B, Kopera L, Melišek T and Nielsch K 2020 *J. Alloys Compd.* **829** 154543

[39] Mroczek Z, Morawski A, Czujko T, Karaboga F, Akdogan M, Zaleski A J, Malecka M, Cetner T, Yetis H, Gajda D and Belenli İ 2019 *J. Alloys Compd.* **776** 636

[40] Grivel J C , Abrahamsen A and Bednarčík J 2008 *Supercond. Sci. Technol*. **21** 035006

[41] Chen S K, Yates K A, Blamire M G, MacManus and Driscoll J L 2005 *Supercond. Sci. Technol*. **18** 1473

[42] Akdogan M, Yetis H, Gajda D, Karaboga F, Rogacki K, Morawski A and Belenli İ 2017 *J. Alloys Compd.* **702** 399